Open access • Journal Article • DOI:10.1029/JD095ID03P02047

Stabilization functions of unforced cumulus clouds : their nature and components

Jorge A. Ramírez, Rafael L. Bras, Kerry Emanuel

Institutions: Marshall Space Flight Center, Massachusetts Institute of Technology

Published on: 28 Feb 1990 - Journal of Geophysical Research (John Wiley & Sons, Ltd)

Topics: Convective available potential energy, Free convective layer, Atmospheric convection, Cloud physics and Convective instability

JOURNAL OF GEOPHYSICAL RESEARCH, VOL. 95, NO. D3, PAGES 2047–2059, FEBRUARY 28, 1990

Stabilization Functions of Unforced Cumulus Clouds: Their Nature and Components

JORGE A. RAMIREZ,[1] RAFAEL L. BRAS, AND KERRY A. EMANUEL

Massachusetts Institute of Technology, Cambridge

Is there an intrinsic characteristic of free moist atmospheric convection that induces a particular type of space-time structure within cloud fields? What is the expected nature of the spatial distribution of cumuli within unforced cumulus cloud fields? This paper is one of two in this collection that addresses these fundamental questions. The thermodynamic effects of convection are quantified as functions of changes of convective available potential energy (CAPE) induced by the convective overturning. The time rate of change of CAPE is parameterized in terms of a kernel of influence or stabilization function. A three-dimensional cloud model is used to infer and quantify stabilization functions by performing single-cloud experiments. Measured stabilization functions are positive everywhere, decreasing away from the cloud center. Stabilization functions are decomposed into various thermodynamic contributions involving pressure, temperature, and moisture changes in the boundary layer and above. It is observed that the major contribution to the environmental stabilization comes from the drying of the planetary boundary layer induced by subsidence. The thermodynamic effect of nonprecipitating and precipitating convection is to reduce CAPE in the surrounding environment and hence reduce the conditional probability of further convection nearby. A new hypothesis with respect to the spatial distribution of cumuli is postulated. The inhibition hypothesis states that, under completely homogeneous external conditions and assuming a spatially random distribution of cloud-trigering mechanisms, the spatial distribution of cumuli in the resulting cloud field must be regular, as opposed to either random or clustered, because cumulus clouds tend to reduce the available energy for convection, thereby inhibiting further convection nearby.

1. INTRODUCTION

One of the most difficult tasks in modeling precipitation is describing its space-time variability. Convective processes are responsible for most of this variability. Thus cumulus clouds and their effects on the surrounding thermodynamic environment must be understood. Issues that must be addressed include (1) what is the interaction between atmospheric convection and the large-scale environment and how can it be characterized, (2) what is the relationship between the characteristics of this interaction and the observed nature of the spatial distribution of cumuli, and (3) how can these facts be incorporated into physically based hydrologic precipitation models?

Atmospheric convection is a very complex process. Many dynamical, thermodynamical, and microphysical interactions and processes take place during convective overturning, not the least of which is latent heat release. All these phenomena must have a bearing on the time and space evolution of convective activity. Furthermore, large-scale processes associated with initial conditions and imposed boundary conditions like topography, radiative effects, heat and moisture surface fluxes, and wind characteristics will also be important factors in determining the evolution of convection, not only because of their interactions with convection itself, but more important, because of their own inherent space-time variability.

Is there an intrinsic characteristic of free moist atmospheric convection that tries to induce a particular type of space-time structure? Specifically, what is the expected nature of the spatial distribution of cumuli within unforced cumulus cloud fields? This paper is one of two in this collection [*Ramirez and Bras*, this issue] which tries to obtain answers to this fundamental question. In order to do so the thermodynamic effects of convection must be isolated from all other possible external influences that would otherwise be present in nature. This paper deals with the quantification of the thermodynamic effects of convection. The definition of spatial grouping characteristics is dealt with by *Ramirez and Bras* [this issue].

The following sections will quantify the thermodynamic influence of a convecting region on the surrounding atmosphere. This influence will be measured in terms of changes of convective available potential energy (CAPE). Convectively induced changes in CAPE will be parameterized in terms of a kernel of influence or stabilization function whose time rate of change is defined in the next section.

In order to infer and quantify the defined kernel, a three-dimensional cloud model is used. Single-cloud experiments are designed and performed to study thechange of CAPE induced by convection. The observed behavior is explained by decomposing the resulting kernel function into various thermodynamic contributions involving pressure, temperature, and moisture changes in the boundary layer and above.

It is observed that the integrated time rate of change of CAPE is negative everywhere, becoming less negative away from the cloud center. The reduction of CAPE extends over several cloud radii and is long lasting. This reduction of CAPE continues to exist after cloud dissipation for times comparable to cloud development time. The thermodynamic effect of nonprecipitating and precipitating convection is to reduce CAPE in the surrounding environment and hence reduce the conditional probability of further convection

[1]Now at Universities Space Research Association, NASA Marshall Space Flight Center, Huntsville, Alabama.

Paper number 89JD02750.
0148-0227/90/89JD-02750$05.00

developing nearby. This is called the inhibition hypothesis. Building on literature on inhibitory spatial processes, this result implies that the thermodynamic effects of convection favor a regular spatial distribution, characterized by a tendency to maintain a minimum distance between clouds. The objective definition of regularity and the test and verification of the inhibition hypothesis are carried out in the accompanying paper [*Ramirez and Bras*, this issue].

2. Convective Instability and Stabilization Kernel

Unforced cumulus clouds develop as a result of the convective instability of the environment. An integrated measure of the degree of atmospheric convective instability is the CAPE of an arbitrarily selected individual air parcel, usually from the well-mixed planetary boundary layer (PBL). This measure is customarily expressed as a function of buoyancy $B(\ )$ as

$$\text{CAPE} = A(\cdot, \cdot) = \int_{\text{LFC}}^{\text{LNB}} B(\cdot, \cdot)\, dz = \int_{\text{LFC}}^{\text{LNB}} g \frac{\theta_{vp} - \theta_{va}}{\theta_{va}}\, dz \qquad (1)$$

where LNB and LFC stand for level of neutral buoyancy and level of free convection, respectively, and θ_{vp} and θ_{va} are virtual potential temperatures of parcel and ambient air, respectively.

The time rate of change of CAPE represents the net effect of stabilizing and destabilizing atmospheric processes. In general, the change in CAPE can be decomposed as due to cumulus convection processes on the one hand, and to all other processes on the other hand.

The main assumptions of the work reported here are that the effects of cumulus convection on the surrounding thermodynamic environment can be defined by a stabilization function in the time and space domains, that the stabilization function can be expressed as a function of the time rate of change of convective available potential energy, and that the spatial distribution of the convection-induced stabilization, that is, the nature of the stabilization kernel in the space domain, is an important factor in determining how cumuli are spatially distributed within unforced cumulus cloud fields. The stabilizing effect of a single cumulus cloud on its surrounding thermodynamic environment is then written as

$$\frac{dA(\bar{x}, t)}{dt} = -K^*(\bar{x}, \bar{y}, t)C(\bar{y}, t) \qquad (2)$$

where $\bar{x}$, $\bar{y}$ are horizontal spatial coordinates, $K^*(\ )$ is a kernel yielding the stabilization at point $\bar{x}$ due to a unit of convection at point $\bar{y}$ and time t, and $C(\ )$ is a function describing the degree of convective activity at point $\bar{y}$. When (2) is applied to an ensemble of clouds, it becomes a generalized convolution between the stabilization function and the convective activity function. *Arakawa and Schubert* [1974] used an analogous representation but in the spectral domain. In a conceptual study of the causes of clustering, *Randall and Huffman* [1980] introduced an integrated version of (2) which they applied to individual clouds.

If (2) is integrated over time since the beginning of the cloud, the cumulative (total) effect of the cloud up to that time can be expressed as a function of a cumulative stabilization function $K(\ )$ as

$$K(\bar{x}, \bar{y}, t) = \frac{1}{\Delta t}\int_{t_0}^{t} K^*(\bar{x}, \bar{y}, t')C(\bar{y}, t')\, dt' = -\frac{\Delta A(\bar{x}, \bar{y}, t)}{\Delta t} \qquad (3)$$

where $\Delta t = (t - t_0)$ is the time elapsed since the cloud birth, t_0.

3. Numerically Generated Clouds: Model and Experiments

3.1. *Model*

A major obstacle to testing any hypothesis on cumulus clouds is the quality and quantity of available observational data, particularly at scales which are comparable to the cumulus convection scale itself. The cloud-induced environmental stabilization is important at precisely the cloud scale. Thus it is necessary to resort to other ways of obtaining "pseudo-observational" data. The use of a numerical model for three-dimensional simulation of cumulus convection overcomes some of the data limitations. Clearly, the results of analyses based on simulated data are valid only insofar as the validity of the cloud model used. Present convection models, although limited in their capabilities, are the only tools available. Their use can be and has been of great help in understanding the behavior of atmospheric processes. The model chosen in this work is a limited-area, three-dimensional, finite difference model. The model is nonhydrostatic. It uses the anelastic approximation and solves the equations of motion and the first law of thermodynamics in a domain with irregular lower boundary. The model has been developed by *Clark* [1977, 1979] and his collaborators at the National Center for Atmospheric Research (NCAR) [e.g., *Clark and Hall*, 1979; *Clark and Gall*, 1982; *Clark and Farley*, 1984; *Hall*, 1980; *Smolarkiewicz and Clark*, 1985]. (See Appendix A for model details.)

3.2. *Cloud Experiments*

Four single-cloud experiments, as described in Table 1, were designed and performed in order to isolate and measure the effects of individual clouds on their surrounding thermodynamic environment. Both purely thermodynamic (e.g., warm bubble) and purely dynamic perturbations were used to initialize convection. Since a purely thermodynamic initialization affects the very same thermodynamic fields which need to be measured in order to compute A( ) and K( ), nondivergent momentum perturbations were used to initialize clouds R1TEST and S1TEST. Only results from clouds R1TEST and S1TEST are discussed below. Although both S1TEST and R1TEST were initialized with a momentum perturbation of equal energy input, the region affected by the perturbation was much larger for experiment S1TEST.

Neither surface fluxes (e.g., evaporation from the ground, surface heating) nor radiative effects is included in the simulation of isolated clouds. No large-scale forcing is provided, either. The initial conditionally unstable atmospheric state is allowed to evolve as convection takes place. By providing no large-scale forcing, the thermodynamic effects of convection are isolated. Convection is induced by a nondivergent, instantaneous momentum perturbation whose integrated energy input is barely enough to overcome the stable stratification of the PBL. Initial thermodynamic

TABLE 1. Single-Cloud Experiments: Description of Simulation Characteristics

	J1TEST	P1TEST	R1TEST	S1TEST
Boundary conditions	periodic	radiation	radiation	radiation
Initialization	warm bubble	warm bubble	momentum perturbation	momentum perturbation
Soundings	hydrostatic (ad hoc)	hydrostatic (ad hoc)	Jordan's	Jordan's
Prandtl number	1	1	1/3	1/3
Time step, s	10	10	10	10
Horizontal resolution, km	1.0	1.0	1.0	1.0
Vertical resolution, km	0.5	0.5	0.5	0.5
Domain size (X, Y, Z)	62 , 62, 30	62 , 62, 30	62 , 62, 30	62 , 62, 30
Cloud duration, s	>1200	>7200	7200	4800
Simulated time, s	1200	7200	9000	6600

soundings of temperature and water vapor mixing ratio for both R1TEST and S1TEST are identical (Figure 1) and correspond to *Jordan*'s [1958] mean tropical soundings for the hurricane season. The initial atmospheric state is windless. Nevertheless, convection-induced large-scale circulations are included and accounted for.

Table 1 summarizes the main simulation characteristics of the single-cloud experiments with respect to domain size, spatial and temporal resolution, initial soundings, boundary conditions, length of simulation, and type of initialization.

In computing stabilization kernels for clouds R1TEST and S1TEST, both dilute and undilute ascent cases were considered. Mixing is defined in terms of the fractional rate of entrainment, λ, which gives the fraction of the total mass of the parcel gained through a vertical displacement dz. (See Appendix B for details on the mixing process.) Dilution by entrainment was achieved by assuming isobaric mixing and conservation of total water mixing ratio and moist static energy. Mixing will in general reduce both the moist static energy of the parcel and its total water mixing ratio. Parcel buoyancy is drastically reduced as a result. Entrainment significantly reduces the available energy for convection as compared with the undilute case. For isolated parcels the entrainment process represents the only mechanism through which a feedback can be established between PBL parcels and existing clouds.

4. THERMODYNAMIC INFLUENCE

4.1. *Observed General Thermodynamic Effects*

The initial thermodynamic conditions for cloud experiments R1 and S1 are shown in Figure 2*a*. Buoyancy, potential temperature, virtual potential temperature, and water vapor mixing ratio are shown. The solid line corre-

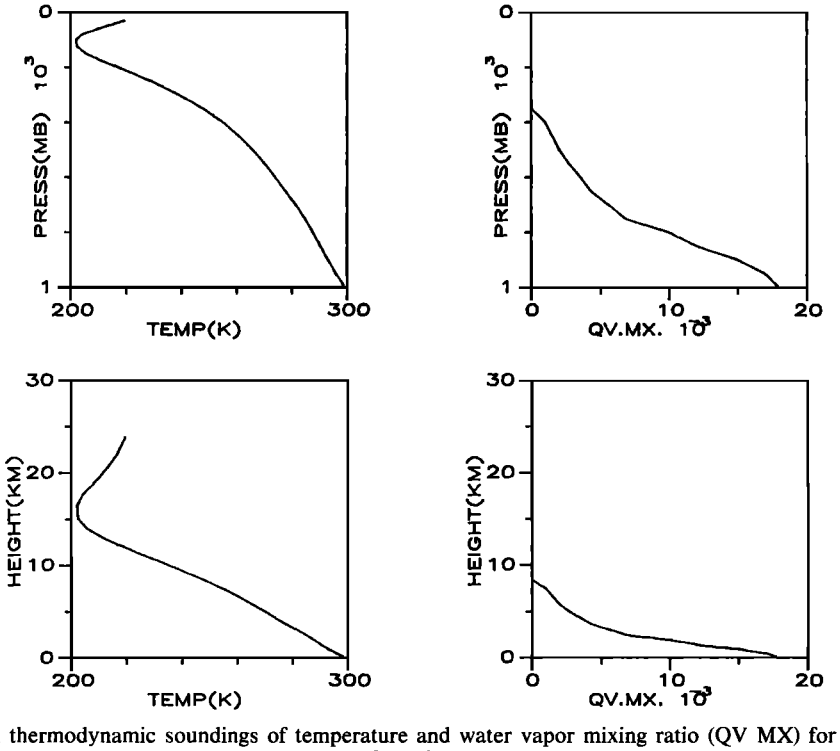

Fig. 1. Initial thermodynamic soundings of temperature and water vapor mixing ratio (QV MX) for R1TEST and S1TEST.

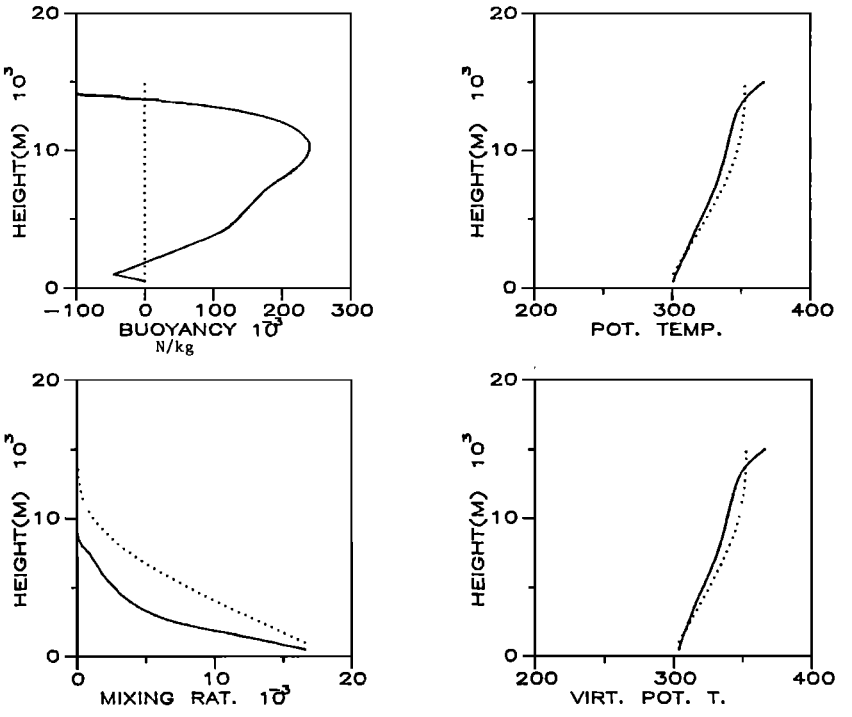

Fig. 2*a*. Initial thermodynamic soundings for R1TEST and S1TEST. Temperatures are in degrees Kelvin. No mixing.

sponds to the atmospheric soundings, and the dotted line to those of a surface parcel lifted adiabatically. Also included is the buoyancy function for the surface parcel, compared with a neutrally buoyant parcel. Similarly, Figures 2*b* and 2*c* show the corresponding thermodynamic soundings at the end of the respective clouds. These figures correspond to soundings representative of points within the cloud itself.

The following effects are immediately apparent when comparing initial and final thermodynamic states.

1. Water vapor mixing ratios have been redistributed. The PBL mixing ratio has been significantly lowered, while that of the upper ambient air has been increased. This moisture redistribution is more pronounced for R1TEST than for S1TEST.

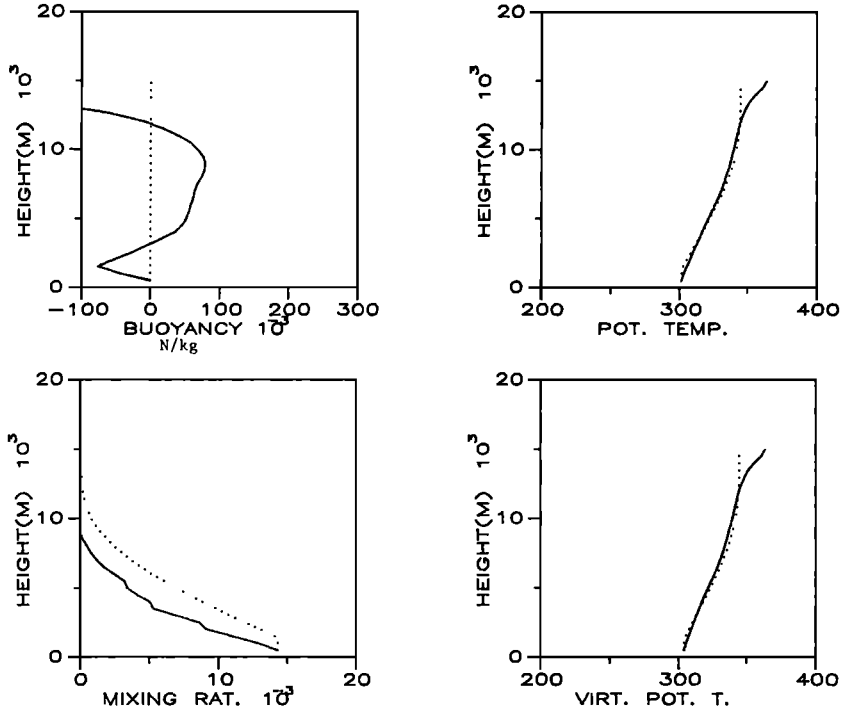

Fig. 2*b*. Thermodynamic soundings for experiment R1TEST 120 min after cloud initiation. Temperatures are in degrees Kelvin. No mixing.

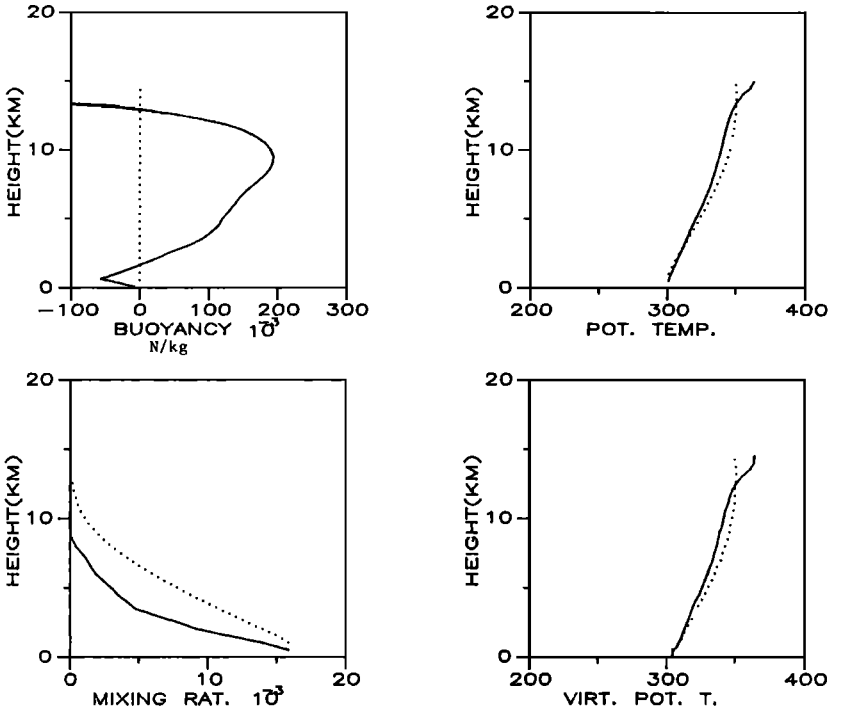

Fig. 2c. Thermodynamic soundings for experiment S1TEST 80 min after cloud initiation. Temperatures are in degrees Kelvin. No mixing.

2. Neither R1TEST nor S1TEST affects, in an appreciable manner, the distributions of potential temperature or of virtual potential temperature of the ambient air. However, the induced changes in surface thermodynamic conditions lead to pronounced effects on the parcel soundings. This effect is more noticeable for cloud R1. The parcel soundings show a decrease in the rate of increase of virtual potential temperature with height, and reach the dry adiabatic state at a lower height.

3. All these effects combine to produce a net stabilization which is of considerable magnitude, as can be elicited from the strong reduction in CAPE and the increase in the negative area.

The most conspicuous effect is a reduction in the water vapor mixing ratio of the PBL while the surface temperature remains very close to the initial temperature. This results in a net reduction of CAPE for the surface parcel and, consequently, a net stabilization of the environment.

4.2. *Inferred Stabilization Kernels*

The time evolution of the stabilization kernel is illustrated in Figure 3 for both clouds R1 and S1 as well as for undilute ($\lambda = 0.0$ km^{-1}) and for dilute ($\lambda = 0.2$ km^{-1}) ascent. Undilute ascent implies parcel air is not allowed to mix with ambient air. For the R1 cloud the dashed lines represent the kernel at 5 min, the dotted lines at 60 min into the cloud evolution, and the solid lines at 150 min after cloud initiation and 30 min after cloud death. For the S1 cloud the dashed lines represent kernels at 5 min after cloud initiation, the dotted line at 40 min, and the solid lines at 110 min after cloud initiation and 30 min after cloud death. These times are typical of cloud initiation, middle, or mature stages and cloud death. A three-dimensional plot of the stabilization function 80 min into S1TEST is also shown in Figure 4. Kernels are computed according to (3). It is clear that the net effect of convection is stabilizing. The spatial distribution of the stabilizing effect decreases with distance from a maximum at the cloud. The magnitude of this stabilization depends on the intensity of the cloud. The R1 cloud produces a 70% stabilization at its center as opposed to only 37% for the S1 cloud. When a fractional rate of entrainment of 0.2 km^{-1} is assumed for parcel ascent, the stabilization kernel at the end of the cloud shows total stabilization (100% reduction in CAPE) to convection for both clouds. For the case of dilute ascent the presence of inertia-gravity waves is rather conspicuous, especially for the earlier times into the cloud evolution. The measured stabilization kernels change very little during the last half of their respective cloud durations, and even 30 min after cloud death, they remain practically unchanged. These results are typical of all simulated clouds, including those initialized with thermodynamic perturbations (J1TEST and P1TEST in Table 1). These stabilization functions are qualitatively similar to the distributions of liquid buoyancy determined by *Bretherton* [1987] in his study on "linear" nonprecipitating convection. In fact, as can be clearly seen from (1) and (3), the stabilization function used here represents an integrated measure of the convectively induced changes in parcel buoyancy. Results of this work, and of Bretherton's, indicate that buoyancy and, consequently, CAPE are reduced around a cloud, and as will be shown in the following section, this is a direct consequence of the adiabatic warming and drying induced by subsiding air.

4.3. *Kernel Components*

Two major components contribute to the definition of the stabilization kernel. The first is the total change in the ambient thermodynamic conditions. The second is the total change in

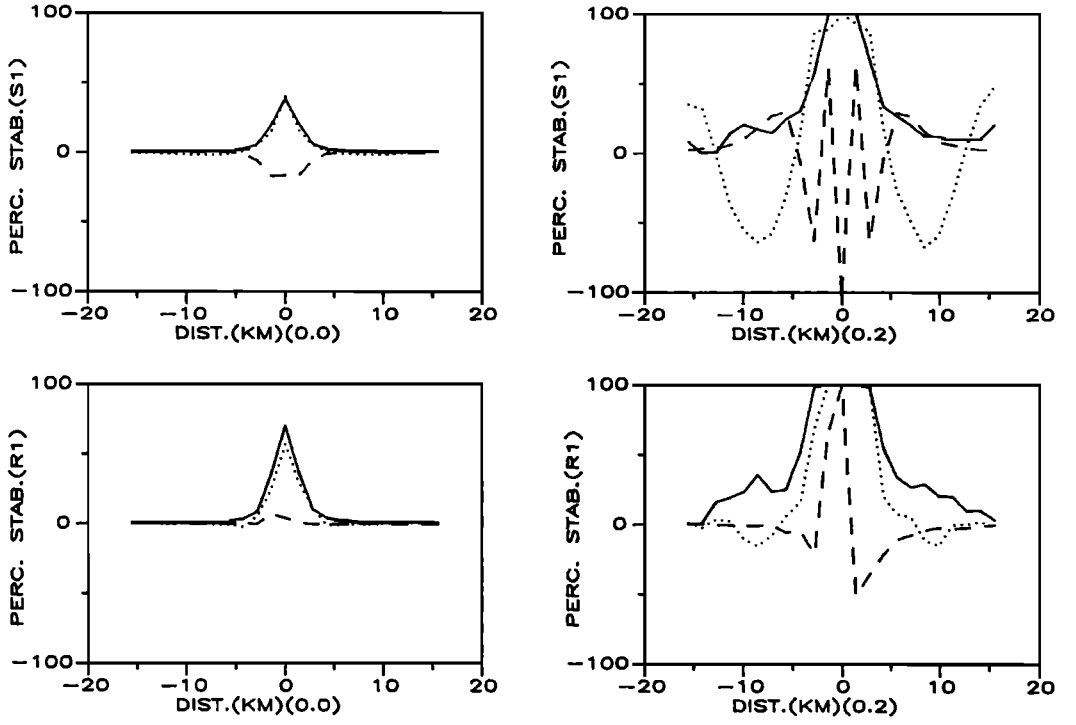

Fig. 3. Stabilization functions for clouds R1TEST and S1TEST. Stabilization functions are given as percent stabilization. Entrainment coefficients are indicated in parentheses.

the parcel thermodynamic conditions, which are in turn determined by the PBL initial conditions and, in the case of mixing, also by the ambient virtual potential temperature. As defined, the stabilization kernel should be decomposable into a PBL-change component and an upper-air-change component. These components were computed for the case of undilute (nonentraining) moist adiabatic ascent [*Ramirez*, 1987]. They refer to the different physical quantities that define the thermodynamic state of both the parcel and the environment. As indicated in Table 2 the main contribution to the stabilization kernel comes from changes in the PBL thermodynamic conditions as they affect the corresponding parcel soundings. In particular, the moisture reduction within the PBL produces the most significant contribution to the net stabilization, as expressed by term 3 in Table 2 (see Appendix C for details on kernel components). The relative contribution of each thermodynamic component to the stabilization kernel is shown in Figures 5*a* and 5*b*. The corresponding total changes in temperature, pressure, and moisture for the surface parcel are shown in Figure 5*c*. Term 1 implies a net destabilization which can only come about if the parcel's initial temperature has increased. Term 3 implies a net stabilization, which in this case can only be produced by a decrease in the initial moisture conditions of the parcel. Large-scale subsidence around a cloud, as a result of large-scale circulations induced by conservation of mass requirements, produces warming and drying of the PBL by mixing initially dry, upper environmental air. Results of these experiments indicate that the stabilizing effect of subsidence is the most important contribution to the total stabilization function.

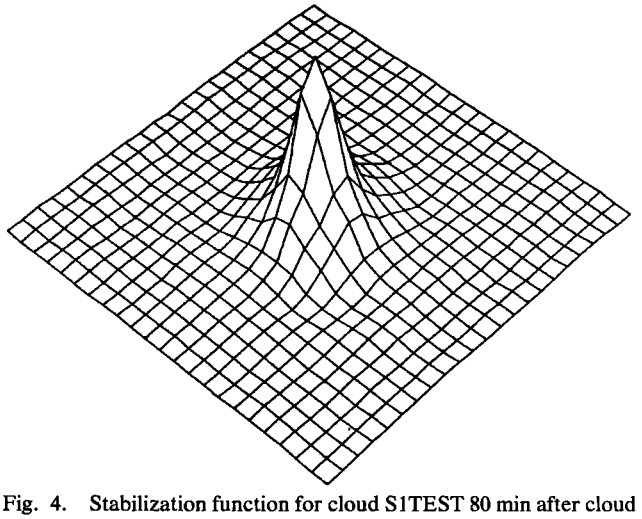

Fig. 4. Stabilization function for cloud S1TEST 80 min after cloud initiation. No mixing.

Discussing possible explanations for the nature of the observed spatial distribution of clouds, *Randall and Huffman* [1980] argue that stabilization functions with relative minima at the cloud (diplike) would account for the assumed clustering, in contrast to stabilization functions with maxima at the cloud (peaklike). A clustering tendency for clouds would require a relative destabilizing effect near regions of active convection. This implies that the stabilization induced by convection must increase away from the cloud center or be negative (destabilizing) near the cloud. It is shown below that dip profiles are feasible only if there is an external forcing that maintains the PBL thermodynamic conditions nearly constant throughout convective overturning, a condition that would be hard to achieve.

Figure 6 shows the evolution of the parcel buoyancy function for cloud R1 (similar results are available for cloud S1). The initial PBL thermodynamic conditions of the parcel are artificially held constant in the computations so as to be

TABLE 2. Stabilization Kernel Components for Simulated Clouds

PBL Components			Ambient Air Components		
Term	d(PBL)	Stabilization, %	Term	d(Ambient Air)	Stabilization, %
		S1TEST			
1	$d \ln T_B^0$	−5.19	6	$d \ln T_a$	2.71
2	$d \ln p^0$	−0.08	7	$d \ln p$	−0.01
3	$d(q_p^0/T_{ps}^0)$	52.40	8	$d \ln (1 + \gamma q_a)$	0.49
4	$d(q_{ps}/T_p)$	−15.40			
5	$d \ln (1 + \gamma q_p)$	1.13			
Total, %		32.86			3.19
		R1TEST			
1	$d \ln T_B^0$	−8.86	6	$d \ln T_a$	−0.43
2	$d \ln p^0$	−0.01	7	$d \ln p$	−0.01
3	$d(q_p^0/T_{ps}^0)$	110.70	8	$d \ln (1 + \gamma q_a)$	1.35
4	$d(q_{ps}/T_p)$	−37.43			
5	$d \ln (1 + \gamma q_p)$	2.62			
Total, %		67.02			0.91

For the S1TEST the decomposed total is 36.05% and the computed total is 40.1%. For the R1TEST the decomposed total is 67.93% and the computed total is 70%.

consistent with the condition mentioned above. Surface fluxes of heat and moisture are thus simulated. Four different values of the fractional rate of entrainment are used, namely, 0.0, 0.05, 0.10, and 0.15 km^{-1}. These values are indicated in parentheses at the bottom of each figure. The solid line corresponds to the initial condition at cloud initiation, the dotted line to midway into the cloud life, and the dashed line to conditions at cloud death. For undilute ascent (entrainment coefficient equal to zero), the amount of available convective energy remains practically unchanged. Since in this case the PBL conditions are being held constant, the only source of stabilization must come from an increase in the ambient virtual potential temperature. However, CAPE is relatively insensitive to thermodynamic changes aloft, as shown in Figure 5 and Table 2.

When dilute ascent is being considered, there is less available convective potential energy than for undilute ascent, at all times. This reduction in CAPE increases with increasing fractional rate of entrainment, as expected. Significantly though, for a fixed entrainment rate, the amount of convective available potential energy with respect to the surface parcel initially increases with time and then tends to relax back to the original CAPE, toward the end of cloud activity. Consequently, as a function of CAPE and for this

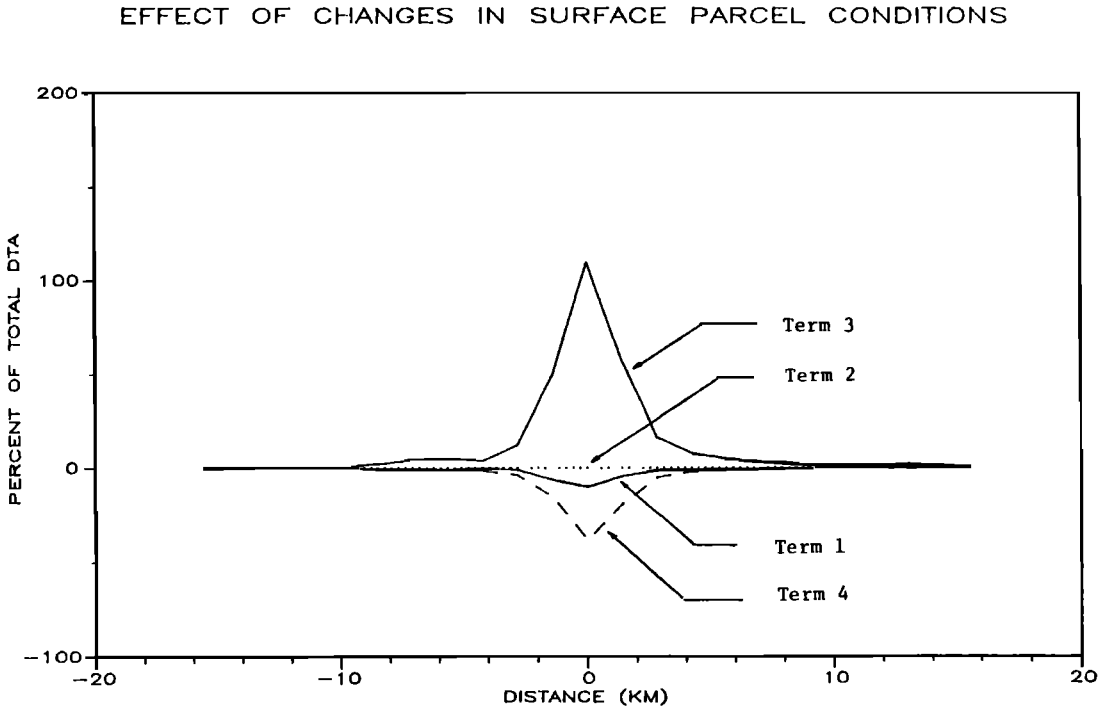

Fig. 5a. Components of stabilization function for cloud R1TEST. Contributions from changes in surface parcel conditions.

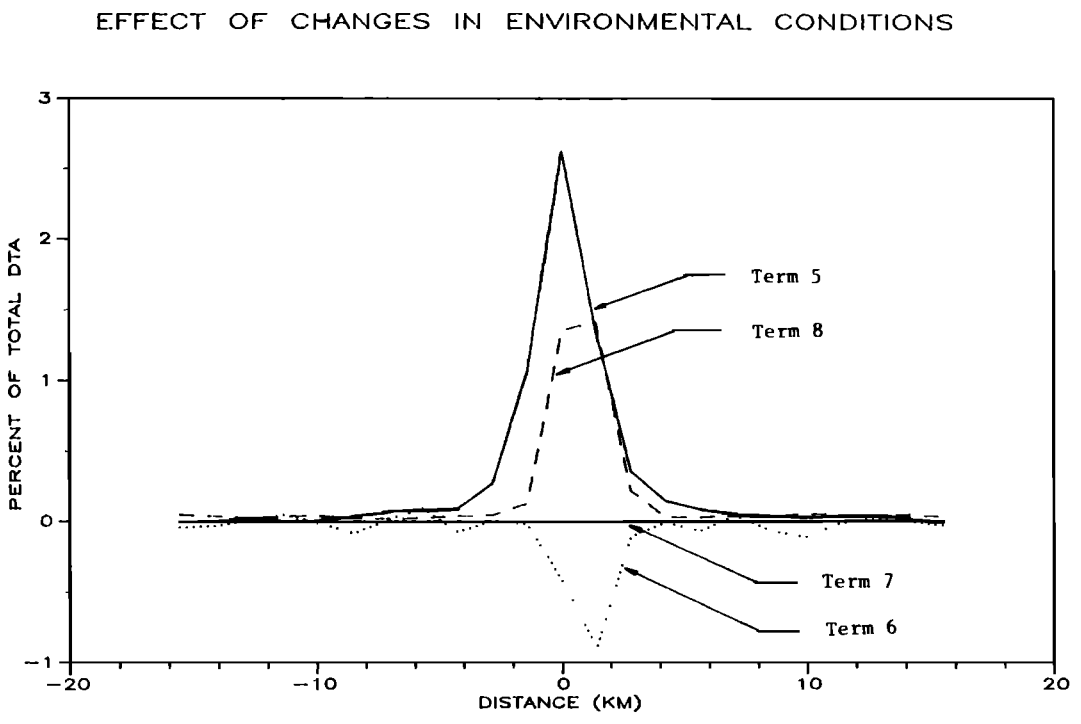

Fig. 5*b*. Components of stabilization function for cloud R1TEST. Contributions from changes in environmental conditions.

particular parcel, there has been a net destabilization, apparently induced by the convection process itself and manifested in a net increase of available CAPE. (Keep in mind that in this experiment, PBL properties are held constant, hence mimicking an external forcing.) The net change in CAPE for dilute ascent is sensitive to the fractional rate of entrainment and, through it, to the thermodynamic changes in the upper air conditions. This is illustrated in Figure 7, which shows the time evolution of CAPE at the cloud center, as the mixing coefficient is allowed to vary from 0.05 to 0.2 km^{-1}. CAPE increases with time, indicating a net environmental destabilization to convection. This destabilization has apparently been brought about by convection itself, and it is a reflection of the fact that during cloud development,

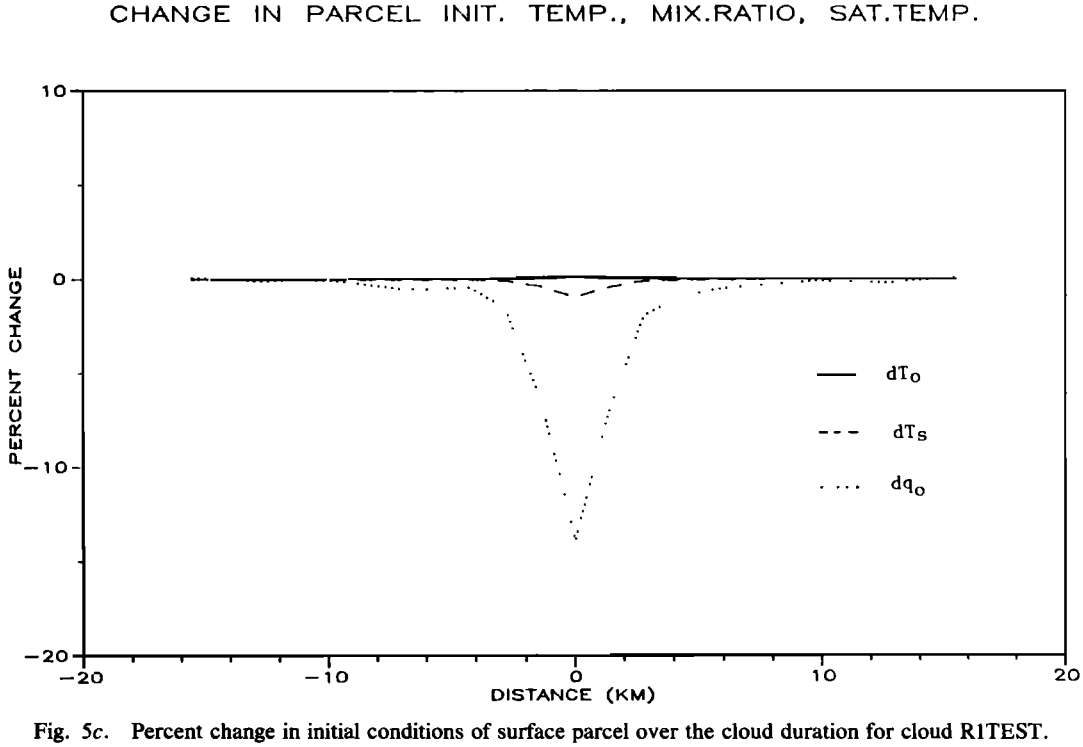

Fig. 5*c*. Percent change in initial conditions of surface parcel over the cloud duration for cloud R1TEST.

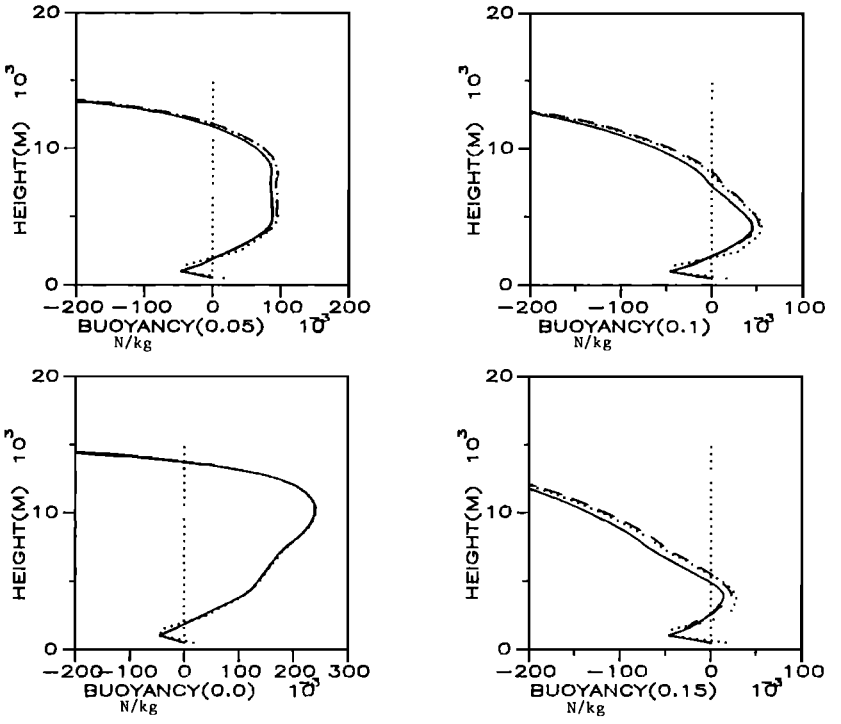

Fig. 6. Effect of mixing on the buoyancy function for cloud R1TEST. Entrainment coefficients are indicated in parentheses (0.0, 0.05, 0.1, and 0.15).

ascending parcels will encounter progressively moister upper air conditions, while the initial parcel conditions remain unchanged. Toward the end of the cloud, although the net effect is manifested as a net destabilization ($dA(\ ) > 0$), the instantaneous rate of change of CAPE is negative, that is, stabilizing. Thus, although the moisture anomaly aloft, introduced by convection, induces a relatively more unstable environment with respect to a surface parcel, this is so only because the surface parcel initial conditions are maintained constant. The net increase of CAPE is a reflection of the energy added to the system by fixing PBL thermodynamic conditions. Consequently, the relative destabilization is not the intrinsic result of convective processes but of large-scale forcing that holds PBL conditions constant.

5. Stabilization Kernels: Discussion

Several important points must be stressed from the results presented above. First, a stabilization kernel defining the thermodynamic effects of convection on the environment can indeed be defined. These kernels have been shown to be robust measures (unique and persistent nature) of the environmental stabilization induced by convection. Thus they can be used to parameterize simple precipitation models

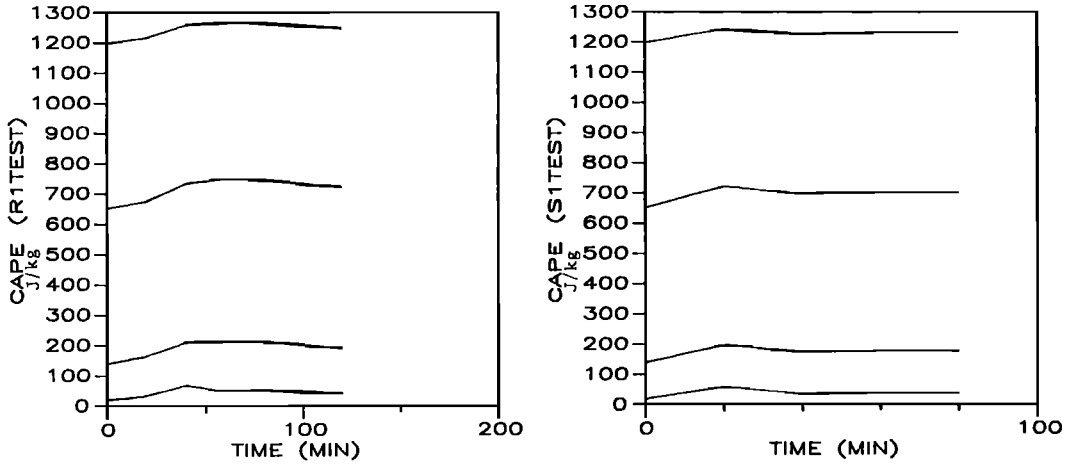

Fig. 7. Time evolution of CAPE for cloud RITEST under constant PBL conditions. Entrainment coefficients are 0.05, 0.1, 0.15, and 0.2. The lowest curve corresponds to entrainment rate of 0.2.

(e.g., for use in hydrology). Inferred kernels, obtained from simulated clouds, show spatial distributions of stabilization which are in agreement with qualitative conceptual arguments based on the expected dynamics of convection [*Ramirez*, 1987]. Both conceptual arguments and observed kernels differ from those that have been suggested in the literature. The stabilization functions represent the fundamental character of the cumulus-scale large-scale interaction during free convective overturning.

Second, the spatial distribution of the stabilization induced by convection has been shown to be maximum at the cloud and to decrease to zero with distance away from the cloud. This contrasts with the kernels that are suggested in the meteorology literature which are of the dip type [*Randall and Huffman*, 1980]. No evidence was found that indicated the existence of dip type stabilization functions in the simulated clouds.

Third, the thermodynamic effects of unforced convection, as measured by the stabilization function, are of finite areal extent. In terms of horizontal cloud size as described by cloud radius, these effects extend out to several cloud radii. This fact is also in qualitative agreement with results by *Bretherton* [1987, 1988] on the extent of the subsidence radius.

Finally, it was also shown that if the PBL thermodynamic conditions are maintained constant, convection-induced environmental destabilization is feasible, although not likely. This offers the possibility of obtaining dip profiles in real atmospheric convection if, for example, some large-scale forcing were acting to maintain constant both the moisture supply and the temperature of the PBL.

6. Cloud Distributions: Inhibition Hypothesis

Stabilization profiles as well as the spatial distribution of cumuli within cloud fields are manifestations of a fundamental property of the convection process that produces them. Observed stabilization functions indicate that convection reduces the available potential energy for further convection. The conditional probability of cloud occurrence in the neighborhood of an existing cloud is reduced with respect to the unconditional probability. The convection process is inhibitory of further convection [*Ramirez*, 1987].

Randall and Huffman [1980] have suggested that the spatial distribution of cumulus clouds, which they assume to be clustered, is the consequence of a stabilization function of dip type, which they associated with a so-called mutual protection hypothesis. However, as discussed above, the induced stabilization reduces the likelihood of convection nearby. Assuming that convection has no effect on the distribution of cloud-triggering mechanisms (CTMs) and given that convection reduces the buoyancy, and thus the energy available for convection everywhere, a given perturbation (CTM) may not produce a cloud where it would have otherwise if convection had not depleted the available CAPE. Convection inhibits further convection nearby. Within this framework, a cloud process resulting from a random population of CTMs should appear as an inhibition process. Clouds will tend to be surrounded by cloud-free areas which correspond to the regions of influence of their stabilization functions. If the density of CTMs is such that clouds will compete for the limited supply of CAPE, the resulting spatial distribution of clouds should be gridlike (regular) as opposed to clustered. (Objective definitions and measures of these types of spatial distributions are introduced by *Ramirez and Bras* [this issue].)

A new hypothesis is now postulated with respect to the spatial distribution of unforced cumulus cloud fields. The inhibition hypothesis states that in the absence of any other external forcing, except those associated with convection itself, the spatial distribution of cumuli within cumulus cloud fields is not clustered, as proposed in the literature, but should tend toward a regular, gridlike distribution in space. This regularity is the manifestation of the inhibition of further convection which is induced by the reduction of available CAPE. This hypothesis disagrees with currently suggested hypotheses in two ways. On the one hand, the inhibition hypothesis suggests that cumulus cloud fields should be regular. The accepted view is that they are clustered. On the other hand, the inhibition hypothesis implies a reduction in convective activity, while currently proposed hypotheses imply mutual protection against cloud dissipation. A verification of this hypothesis is given by *Ramirez* [1987] and *Ramirez and Bras* [this issue].

7. Summary

Conceptual and numerical evidence supporting the idea of stabilization functions as robust descriptors of the fundamental interaction between cumulus convection and the surrounding environment has been given. Stabilization kernels were decomposed into their thermodynamic components. Contributions due to thermodynamic changes in the PBL were separated from those due to thermodynamic changes in the ambient air. It was shown that the major contribution to environmental stabilization comes from changes in the PBL. The decrease in the PBL water vapor mixing ratio was shown to be responsible for most of the computed stabilization.

The spatial distribution of the environmental stabilization was shown to be maximum at the cloud (peak) and to decrease monotonically to zero with distance away from the cloud. No evidence was found for the existence of dip stabilization functions in the clouds simulated. Diplike profiles were shown to be possible only when the thermodynamic state of the planetary boundary layer is held relatively constant.

A new hypothesis with respect to the spatial distribution of cumuli was suggested. The inhibition hypothesis states that, under completely homogeneous external conditions and assuming a spatially random distribution of cloud-triggering mechanisms, the spatial distribution of cumuli in the resulting cloud field must be regular, as opposed to either random or clustered, because cumulus clouds tend to reduce the available energy for convection, thereby inhibiting further convection nearby. Clearly, the inhibition hypothesis is postulated under very restrictive conditions. Unforced convection, as presented here, implies that mechanisms like wind shear and heterogeneity of surface fluxes are not accounted for. These mechanisms may be the dominant ones in real atmospheric convection. However, the work presented here and by *Ramirez and Bras* [this issue] helps clarify one of the many effects of the very complex convection process.

APPENDIX A: CLOUD MODEL DESCRIPTION

The model chosen is a nonhydrostatic, limited-area, three-dimensional finite difference model. It uses the anelastic approximation and solves the equations of motion and the first law of thermodynamics in a domain with irregular lower boundary. The model has been developed by *Clark* [1977, 1979] and his collaborators at NCAR [e.g., *Clark and Hall*, 1979; *Clark and Gall, 1982; Clark and Farley*, 1984; *Hall*, 1980; *Smolarkiewicz and Clark*, 1985].

The momentum equations for the moist air are expressed as

$$\bar{\rho}\frac{du_i}{dt} + \bar{\rho}f(\delta_{i2}u_1 - \delta_{i1} - u_2) = -\frac{\partial p''}{\partial x_i} + \delta_{i3}\bar{\rho}g\left(\frac{\theta''}{\bar{\theta}} + \gamma g_v'' - \frac{p''}{\beta\bar{p}} - q_c - q_r\right) + \frac{\partial \tau_{ij}}{\partial x_j} \quad \text{(A1)}$$

and the anelastic form of the mass continuity equation as

$$\frac{\partial}{\partial x_i}(\bar{\rho}u_i) = 0 \quad \text{(A2)}$$

which are written in standard tensor notation. Here δ_{ij} is the Kronecker delta function and f is the Coriolis parameter. The velocities u_i for $i = 1, 2, 3$ represent velocities in the conventional x, y, and z directions, respectively. The tensor notation is such that summation is performed on the repeated index over the range 1–3. Finally, τ_{ij} is the Reynolds stress tensor whose parameterization is presented later, and q_v, q_c, and q_r represent the mixing ratios for water vapor, cloud water, and rain water, respectively. The thermodynamic variables are partitioned in three components as follows:

$$\theta = \bar{\theta} + \theta'(x_3) + \theta''(\bar{x}, t) = \theta^0(x_3) + \theta''(\bar{x}, t) \quad \text{(A3)}$$

$$\theta = \bar{\theta}(1 + \theta^*) \quad \text{(A4)}$$

$$\theta^* = (\theta - \bar{\theta})/\bar{\theta} \quad \text{(A5)}$$

$$T = \bar{T}(x_3) + T'(x_3) + T''(\bar{x}, t) = T^0(x_3) + T''(\bar{x}, t) \quad \text{(A6)}$$

$$p = \bar{p}(x_3) + p'(x_3) + p''(\bar{x}, t) = p^0(x_3) + p''(\bar{x}, t) \quad \text{(A7)}$$

$$\rho = \bar{\rho}(x_3) + \rho'(x_3) + \rho''(\bar{x}, t) = \rho^0(x_3) + \rho''(\bar{x}, t) \quad \text{(A8)}$$

$$q_v = q_v'(x_3) + q_v''(\bar{x}, t) = q_v^0(x_3) + q_v''(\bar{x}, t) \quad \text{(A9)}$$

where T, θ, p, and ρ represent temperature, potential temperature, pressure, and density of air, respectively. The components with superscript zero represent the hydrostatic atmospheric conditions, which can also be decomposed into a dry isentropic component, represented by the terms with overbars, and a residual represented by terms with a single prime. Other terms appearing in (A1) are $\gamma = (R_v/R_d) - 1$ and $\beta = C_v/C_p$, where R_v and R_d are the gas constants for water vapor and dry air, respectively, and C_v and C_p are the specific heats at constant pressure for the water vapor and the dry air, respectively.

The subgrid-scale turbulence is parameterized by approximating the Reynolds stress tensor with

$$\tau_{ij} = \bar{\rho}K_M D_{ij} \quad \text{(A10)}$$

where the deformation tensor D_{ij} is defined as

$$D_{ij} = \frac{\partial u_i}{\partial x_j} + \frac{\partial u_j}{\partial x_i} - \frac{2}{3}\delta_{ij}\frac{\partial u_k}{\partial x_k} \quad \text{(A11)}$$

The eddy mixing coefficient for momentum, K_M, is defined as

$$K_M = \frac{(C\Delta)^2}{2^{1/2}}|\text{Def}|\left(1 - \frac{K_H}{K_M}Ri\right)^{1/2} \quad \text{(A12)}$$

if $(K_H/K_M)\,Ri < 0$, and zero otherwise where Def is the total deformation which is defined such that

$$\text{Def}^2 = 1/2\sum_i\sum_j D_{ij}^2 \quad \text{(A13)}$$

and where Δ is an effective grid scale taken as a function of the numerical grid increments, K_H is the eddy mixing coefficient for heat and moisture, C is a constant, and Ri is the local Richardson number defined as

$$Ri = g\frac{\partial}{\partial z}(\theta^* + \gamma q_v - q_c - q_r)/\text{Def}^2 \quad \text{(A14)}$$

The heat and moisture conservation equations are

$$\bar{\rho}\frac{d\theta^*}{dt} = \frac{\bar{\rho}L_v}{C_p\bar{T}}(C_{d1} + C_{d2}) + \frac{\partial}{\partial x_i}\left(\bar{\rho}K_H\frac{\partial\theta^*}{\partial x_i}\right) \quad \text{(A15)}$$

$$\bar{\rho}\frac{dq_v}{dt} = -\bar{\rho}C_{d1} - \bar{\rho}C_{d2} + \frac{\partial}{\partial x_i}\left(\bar{\rho}K_H\frac{\partial q_v}{\partial x_i}\right) \quad \text{(A16)}$$

$$\bar{\rho}\frac{dq_c}{dt} = \bar{\rho}C_{d1} - S_{ac} - S_c + \frac{\partial}{\partial x_i}\left(\bar{\rho}K_H\frac{\partial q_c}{\partial x_i}\right) \quad \text{(A17)}$$

$$\bar{\rho}\frac{dq_r}{dt} + \frac{\partial}{\partial z}(\rho\bar{V}_T q_r) = \bar{\rho}C_{d2} + S_{ac} + S_c + \frac{\partial}{\partial x_i}\left(\bar{\rho}K_H\frac{\partial q_r}{\partial x_i}\right) \quad \text{(A18)}$$

Cloud microphysics is parameterized following Kessler's parameterization. C_{d1} represents the condensation/evaporation rate resulting from diffusional growth of cloud droplets, C_{d2} represents the evaporation rate resulting from evaporation of raindrops in subsaturated air, S_{ac} is the autoconversion transfer rate from cloud water to rainwater, and S_c is the transfer rate from cloud water to rainwater resulting from collection of cloud droplets by raindrops, and $\bar{V}_T$ is a mass-weighted average terminal velocity applicable to the raindrops. The condensation/evaporation rate, C_{d1}, is obtained using the so-called bulk physical assumption in which 100% relative humidity is attempted at every time step during the numerical integration scheme.

APPENDIX B: DESCRIPTION OF MIXING PROCESS

The fractional rate of entrainment, λ, is defined as

$$\lambda = \frac{1}{M}\frac{dM}{dz} \quad \text{(B1)}$$

where M is the mass of the parcel. Isobaric mixing is performed linearly according to

$$dh_p = -\frac{dM}{M}(h_p - h_a) \tag{B2}$$

$$dq_{tp} = -\frac{dM}{M}(q_{tp} - q_{ta}) \tag{B3}$$

where conserved quantities are mixed. In this case the linearly mixed conserved quantities are moist static energy, h, defined as

$$h = C_pT + gz + L_vq \tag{B4}$$

and total water mixing ratio, q_t, defined as

$$q_t = q_v + q_l \tag{B5}$$

Expanding (B2) and assuming hydrostatic conditions, the following equation can be obtained:

$$C_pT_p\left[d\ln T_p - \frac{R_d}{C_p}d\ln p\right] = -L_v\,dq_p - \lambda[C_p(T_p - T_a) + L_v(q_p - q_a)]\,dz \tag{B6}$$

By definition

$$d\ln T_p - \frac{R_d}{C_p}d\ln p = d\ln\theta_p \tag{B7}$$

Substituting

$$d\ln\theta_p = -\frac{L_v}{C_pT_p}dq_p - \lambda\left[\frac{T_p - T_a}{T_p} + \frac{L_v}{C_pT_p}(q_p - q_a)\right]dz \tag{B8}$$

When there is no mixing, and the process under consideration is adiabatic,

$$d\ln\theta = -\frac{L_v}{C_pT}dq \tag{B9}$$

Thus (B8) can be written as

$$d\ln\theta_p^m = d\ln\theta_p^{nm} - \lambda\left[(\theta_p - \theta_a)/\theta_p + \frac{L_v}{C_pT_p}(q_p - q_a)\right]dz \tag{B10}$$

where the superscripts m and nm stand for mixing and no mixing, respectively.

When there is no mixing, that is, when $\lambda = 0$, θ_p is independent of environmental conditions and is determined by the adiabatic process definition. However, when mixing takes place, the situation is radically changed. For normal atmospheric conditions, and with respect to a surface parcel, the bracketed term in (B10) will always be positive above the level of free convection (LFC). Thus, above LFC the rate of increase of θ_p with height is decreased with respect to the undilute ascent case due to mixing. As a result, buoyancy and its associated CAPE are reduced.

Appendix C: Kernel Components

The stabilization kernel is defined in terms of $A(\bar{x}, t)$ as follows:

$$dA(\bar{x}, t) = g\int_{\mathrm{LFC}}^{\mathrm{LNB}}\frac{\theta_{vp}}{\theta_{va}}\frac{d\ln\theta_{vp}}{dt}dz - g\int_{\mathrm{LFC}}^{\mathrm{LNB}}\frac{\theta_{vp}}{\theta_{va}}\frac{d\ln\theta_{va}}{dt}dz \tag{C1}$$

where, in general, $\theta_v = \theta(1 + 0.608q)$. Concentrating on the first term of the right-hand side,

$$\frac{d\ln\theta_{vp}}{dt} = \frac{d\ln\theta_p}{dt} + \frac{d\ln}{dt}(1 + 0.608q_p) \tag{C2}$$

Under conditions of undilute and moist adiabatic ascent,

$$d\ln\theta_p = -\frac{L_v}{C_pT_p}dq_p \tag{C3}$$

The integration interval in (C1) goes from LFC to LNB. Under atmospheric conditions, this implies that the parcel is saturated. Otherwise, assuming adiabatic lifting in a stably stratified atmosphere, if no condensation occurs, the equation,

$$B(\bar{x}, z_{\mathrm{LFC}}, t) = 0 \tag{C4}$$

has no real solution, and LFC does not exist. The equivalent potential temperature, θ_e, can be written as

$$d(\ln\theta_{ep}) = d\left(\ln\theta_p + \frac{L_vq_{ps}}{C_pT_p}\right) = 0 \tag{C5}$$

Equations (C3) and (C5) are valid only above LCL, where the parcel is saturated. Below LCL, and under adiabatic ascent, the following conditions hold:

$$d\ln\theta_p = 0 \tag{C6}$$

and

$$dq_p = 0 \tag{C7}$$

Furthermore, for a given parcel, the saturation temperature, T_{ps}, is also a constant. Then from (C7),

$$\frac{L_v}{C_pT_{ps}^0}dq_p^0 = 0 \tag{C8}$$

Another conserved quantity can then be defined by adding (C6) and (C8) such that

$$d\ln\theta_p^0 + \frac{L_v}{C_pT_{ps}^0}dq_p^0 = 0 \tag{C9}$$

where θ_p^0, q_p^0, and T_{ps}^0 define the parcel PBL thermodynamic conditions, and

$$\ln\theta_p^0 + \frac{L_v}{C_pT_{ps}^0}q_p^0 = \mathrm{const} \tag{C10}$$

By definition, (C5) and (C10) match, and

$$\ln\theta_p = \ln\theta_p^0 + \frac{L_vq_p^0}{C_pT_{ps}^0} - \frac{L_vq_{ps}}{C_pT_p} \tag{C11}$$

which after differentiating and substituting into (C2) yields

$$\frac{d \ln \theta_{vp}}{dt} = \frac{d \ln T_p^0}{dt} - \frac{R_d}{C_p} \frac{d \ln p^0}{dt} + \frac{L_v}{C_p} \frac{d}{dt} \left(\frac{q_p^0}{T_{ps}^0} - \frac{q_{ps}}{T_p} \right) + \frac{0.608}{(1 + 0.608 q_{ps})} \frac{dq_{ps}}{dt} \quad \text{(C12)}$$

Finally, the second term on the right-hand side of (C1) is

$$\frac{d \ln \theta_{va}}{dt} = \frac{d \ln \theta_a}{dt} + \frac{0.608}{(1 + 0.608 q_a)} \frac{dq_a}{dt} \quad \text{(C13)}$$

which can be rewritten as

$$\frac{d \ln \theta_{va}}{dt} = \frac{d \ln T_a}{dt} - \frac{R_d}{C_p} \frac{d \ln p}{dt} + \frac{0.608}{(1 + 0.608 q_a)} \frac{dq_a}{dt} \quad \text{(C14)}$$

Substituting (C12) and (C14) into (C1) yields the stabilization kernel as a function of changes in the thermodynamic conditions of the planetary boundary layer and of changes in upper air conditions.

Acknowledgments. Support for this work was provided in part by the National Science Foundation and the National Aeronautics and Space Administration through grant 8611458-ATM NASA/NSF; by the National Weather Service, Office of Hydrology, through cooperative agreement NA86AA-D-HY123; and in part by the Organization of American States through OAS Fellowship BEGES-83206. Terry Clark and Bill Hall of NCAR provided assistance with the cloud model.

REFERENCES

Arakawa, A., and W. H. Schubert, The interaction of a cumulus cloud ensemble with the large-scale environment, I, *J. Atmos. Sci.*, *31*, 674–701, 1974.

Bretherton, C. S., A theory for nonprecipitating moist convection between two parallel plates, I, Thermodynamics and "linear" solutions, *J. Atmos. Sci.*, *44*(14), 1809–1827, 1987.

Bretherton, C. S., A theory for nonprecipitating convection between two parallel plates, II, Nonlinear theory and cloud field organization, *J. Atmos. Sci.*, *45*(17), 2391–2415, 1988.

Clark, T. L., A small-scale dynamic model using a terrain-following coordinate transformation, *J. Comput. Phys.*, *24*, 186–215, 1977.

Clark, T. L., Numerical simulations with a three-dimensional cloud model, Lateral boundary condition experiments and multicellular severe storm simulations, *J. Atmos. Sci.*, *36*(11), 2190–2215, 1979.

Clark, T. L., and R. D. Farley, Severe downslope windstorm calculations in two and three spatial dimensions using anelastic interactive grid nesting: A possible mechanism for gustiness, *J. Atmos. Sci.*, *41*, 329–350, 1984.

Clark, T. L., and R. Gall, Three-dimensional numerical model simulations of airflow over mountainous terrain: A comparison with observations, *Mon. Weather Rev.*, *110*(7), 766–791, 1982.

Clark, T. L., and W. D. Hall, A numerical experiment on stochastic condensation theory, *J. Atmos. Sci.*, *36*(3), 470–483, 1979.

Hall, W. D., A detailed micro-physical model within a two-dimensional dynamic framework: Model description and preliminary results, *J. Atmos. Sci.*, *37*(11), 2486–2507, 1980.

Jordan, C. L., Mean soundings for the West Indies area, *J. Meteorol.*, *15*, 91–97, 1958.

Ramirez, J., Cumulus clouds: The relationship between their atmospheric stabilization and their spatial distribution, Ph.D. thesis, 429 pp., Mass. Inst. of Technol., Cambridge, 1987.

Ramirez, J., and R. Bras, Clustered or regular cumulus cloud fields: The statistical character of observed and simulated cloud fields, *J. Geophys. Res.*, this issue.

Randall, D., and G. Huffman, A stochastic model of cumulus clumping, *J. Atmos. Sci.*, *37*(9), 2068–2078, 1980.

Smolarkiewicz, P. K., and T. L. Clark, Numerical simulation of the evolution of a three-dimensional field of cumulus clouds, I, Model description, comparison with observations and sensitivity studies, *J. Atmos. Sci.*, *42*(5), 502–522, 1985.

R. L. Bras, Institute of Hydraulic Research, Room 403, University of Iowa, Iowa City, IA 52242.

K. A. Emanuel, Massachusetts Institute of Technology, Cambridge, MA 02139.

J. A. Ramirez, Universities Space Research Association, NASA Marshall Space Flight Center, Mail Code ES44, Huntsville, AL 35812.

(Received November 16, 1988;
revised May 19, 1989;
accepted August 8, 1989.)